ELSEVIER

Journal of Petroleum Science and Engineering 20 (1998) 9–29

JOURNAL OF PETROLEUM SCIENCE & ENGINEERING

Transient aqueous foam flow in porous media: experiments and modeling

O. Fergui, H. Bertin *, M. Quintard

LEPT-ENSAM, University of Bordeaux I, URA CNRS 873, 33405 Talence Cedex, France

Received 19 March 1997; revised 11 February 1998; accepted 11 February 1998

Abstract

Gas injection into reservoirs can be used to increase oil recovery. However, the viscosity and density differences between the injected and displaced fluids can lead to low sweep efficiency. To overcome mobility control problems, gas can be injected in the form of foam to increase its apparent viscosity and improve reservoir sweep efficiency. Our study is focused on transient aqueous foam flow in homogeneous porous media. The experimental apparatus designed for this study consisted on an unconsolidated porous medium, saturated by surfactant-laden water, where nitrogen is injected at a constant flow rate. Pressure drop along the core was monitored, while 2D saturation measurements were performed using a γ-ray attenuation technique. The experiments were analyzed in terms of breakthrough time, liquid recovery, pressure drop evolution along the core, and gas saturation profiles. First, we studied the influence of surfactant concentration. Second, for two fixed values of the surfactant concentration, we studied the influence of gas flow rate. The experiments were interpreted using a foam simulator, including a classical Darcy's law model coupled with a foam bubble population-balance equation to model generation, destruction, and convection of gas bubbles along the porous medium. Physical parameters describing generation and coalescence of foam lamellae have been optimized by a sensitivity study. © 1998 Elsevier Science B.V.

Keywords: porous media; foam flow; experiments; modeling

1. Introduction

Gas drive fluids are used during enhanced oil recovery processes (injection of hydrocarbons gas, nitrogen, carbon dioxide, steam...). The low viscosity of the injected gas and high-density contrast with the displaced fluid is, in many practical situations, the cause of low sweep efficiency due to unstable displacement (viscous fingering) and gravity override. Natural heterogeneity of the reservoir may emphasize these effects.

Since the first studies of Bond and Holbrook (1958) and Fried (1961), gas can be injected in the form of foam in order to increase its apparent viscosity and therefore, achieve a better mobility control during a displacement process.

* Corresponding author. E-mail: bertin@lept-ensam.u-bordeaux.fr

PII S0920-4105(98)00036-9

Foams are used also in several petroleum engineering applications such as matrix acidization (Zhou and Rossen, 1992; Zerhboub et al., 1994), gas blocking for profile control (Hanssen and Haugun, 1991) or drilling operations.

Foams are gas bubbles separated by thin liquid films called lamellae, i.e., the liquid phase is continuous while the gas phase is not. Foams in porous media are distinct from common bulk foams in the sense that when gas enters in the porous structure, the formed bubbles have almost the same characteristic length as the pore bodies.

There is a wide literature on foams in petroleum engineering (see for example the volume edited by L. Schramm, 1994a). Many authors tried to understand and describe foam from the point of views of generation, stability, rheology and propagation. Experimental studies performed with capillary tubes (Hirasaki and Lawson, 1985) showed the pseudoplastic behavior of foam. Microscopic phenomena could be observed using micromodels. Owete and Brigham (1987), using silicon plates, observed the displacement of aqueous surfactant solutions by air as a network of interconnecting films. They showed evidence that liquid and air were trapped in some pores. Chambers and Radke (1991) showed clearly that foam in porous media is not continuous.

Foam displacement in porous media has been extensively studied. Several authors focused their attention on the steady-state determination of relative permeability curves. The main conclusion is that relative permeability to water is almost independent of the presence of surfactant. However, relative permeability to gas is significantly decreased in presence of surfactant. This effect is attributed to the wetting nature of water, and to the large trapped gas saturation. This trapped gas saturation has been measured using gas-phase tracer techniques (Gillis and Radke, 1990; Friedmann et al., 1991). These authors have shown that it could be a very high value (more than 80%). Friedmann and Jensen (1986) described the effect of flow rate on foam in porous media. The authors report experimental results showing the pronounced effect on foam texture, i.e., faster flow rates can produce smaller bubbles than slower flow rates do.

During IOR processes, the flow is obviously time-dependent and, from our point of view, it is necessary to determine the unsteady-state relative permeability curves. Kovscek and Radke (1993) reported experimental results that could be described satisfactorily by a mechanistic model including a population-balance equation.

Our study deals with the injection of gas in unconsolidated porous media saturated by the surfactant-laden solution in the absence of oil. We understand that this last condition is not completely realistic for most petroleum engineering operations, but we believe that, from a mechanistic point of view, it is important to understand the foam flow in porous media before complicating the problem with foam/oil interaction. The reader concerned by this problem can be oriented towards the studies done by Schramm et al. (1990), Manlowe and Radke (1990), Bergeron et al. (1993) and Schramm (1994b), among others.

The experiments described in this paper were performed in a classical petrophysical way, i.e., injecting the gas in the saturated porous medium at a constant rate while measuring the breakthrough time, the liquid recovery, the evolution of pressure drop along the core, and the saturation fields by using a γ-ray attenuation technique. Foam texture is function of surfactant concentration, gas velocity and permeability of the porous medium. By keeping this last parameter constant, we focused our attention on the effects of surfactant concentration and gas flow rate.

The experiments were tentatively interpreted using a classical two-phase flow model with relative permeability curves being estimated from the data. The agreement between experimental data and numerical results was poor, especially, in terms of whole pressure drop fitting. This discrepancy was attributed to the fact that foam viscosity was kept constant in the simulation.

According to the literature, foam texture being admitted as the most important variable in the determination of foam mobility, we used a foam simulator including a classical reservoir simulator coupled with a foam bubble population-balance equation, taking into account the physical parameters that influence the foam texture, namely generation, destruction, and convection of the bubbles. We were able to reproduce most of the characteristic features observed during the foam displacements. This shows that population-balance models are good conceptual models. However, one difficulty already mentioned by previous authors (Friedmann et al.

(1988); Kovscek and Radke (1994)) has to be overcome. Such models require several nonlinear functions describing the foam generation and coalescence, which are difficult to measure. We used the approach of Friedmann et al. (1988) and Kovscek and Radke (1994), in which these properties were extrapolated from simpler mechanistic models.

2. Experiments

2.1. Experimental setup

The experimental set-up, shown in Fig. 1, was designed to study transient foam flow in porous media at ambient pressure and temperature.

The porous medium, made from calibrated pure silica sand (average diameter of particles = 74 10^{-6} m), was packed in a square cross-section experimental cell (Length = 0.17 m, cross-section area = 0.002025 m^2) built of an inert material specially chosen to avoid adsorption and reaction with the surfactant. A new porous medium was prepared for each experiment, the porosity and permeability were found to be constant, equal to 0.4 and 4 Darcy, respectively. The nitrogen gas was injected in the porous medium through a mass-flow controller allowing low gas flow-rate values (0–5 ml/min).

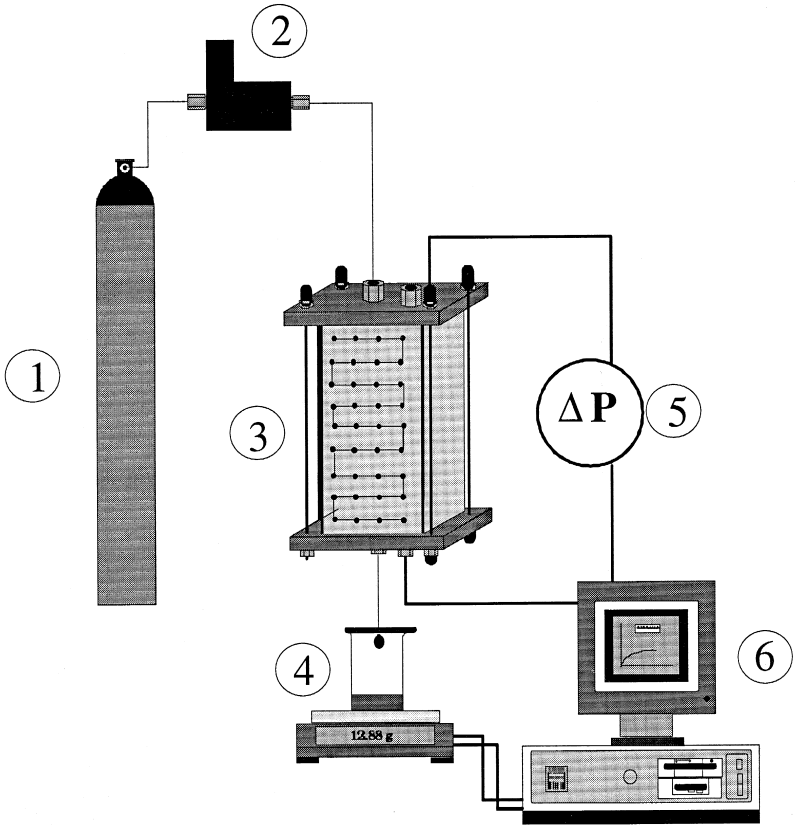

Fig. 1. Experimental setup (1 nitrogen cylinder, (2 gas flow meter controller, (3 experimental cell containing the porous medium, (4 balance, (5 pressure transducer, (6 personal computer).

Porosity and saturation fields during foam flow were measured using a γ-ray attenuation technique. This apparatus is made of a γemitter (Am^{241}, activity = 435 mCi) coupled with a scintillator counter and photo-multiplier. A 2-D displacement apparatus moves the set. Counting is performed by a Canberra™ multi-channel counter. The principle of the measurement is based on the Beer's attenuation law,

$$N = N_0 e^{-\zeta l} \tag{1}$$

where N is the photon counting, N_0 the reference photon counting, ζ the linear attenuation coefficient, and l the width of the medium. The porosity and saturation were measured at the 60 points of a regular net (4×15) represented in Fig. 1.

The porosity, ε is computed using the following equation,

$$\varepsilon = \frac{1}{l\zeta_w} \ln\left(\frac{N_d}{N_w}\right) \tag{2}$$

N_d and N_w are, respectively, the counting of the dry and 100% water saturated medium at the considered point, ζ_w is the attenuation coefficient of water. Air attenuation has been neglected in this equation.

For immiscible two-phase flow we have the relationship,

$$S_w + S_g = 1 \tag{3}$$

where S_w and S_g are the water and gas saturation, respectively, which allows us to compute the water saturation using the following equation,

$$S_w = \frac{1}{l\varepsilon(\zeta_w - \zeta_g)} \ln\left(\frac{N}{N_{wg}}\right) + 1 \tag{4}$$

where ε is the porosity at the measurement location, N_{wg} is the counting of the gas water saturated medium, and ζ_g the attenuation coefficient of gas which is much lower than the water attenuation coefficient and, therefore, can be neglected.

The counting time (20 s/point) allowed us to perform a complete saturation map in less than 30 min. Moreover, the injection rate (0.5 ml/min) was low enough to consider that the saturation map could be considered as an instantaneous picture. The whole pressure drop along the core and water recovery were measured continuously using a differential pressure transducer (0–150 mbar from HBM™) and a precision balance (0.01 g from Mettler™). A PC controlled the displacement apparatus, the photon counting, and recorded all the data.

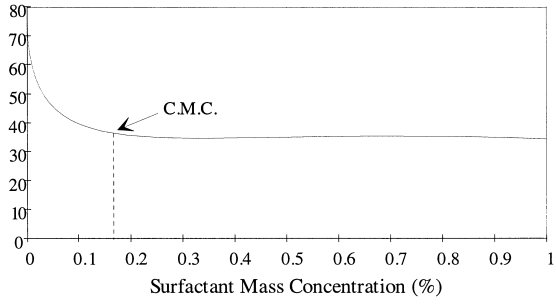

Fig. 2. Surfactant solution interfacial tension vs. surfactant mass concentration.

2.2. Procedure

The surfactant used in this study was an α-olefin sulfonate (C12–C14). The surface tension of several laden surfactant solutions has been measured using the ring method, the critical micellar concentration (CMC) was found equal to 0.17% (mass fraction). The evolution of the interfacial tension as a function of surfactant concentration is given in Fig. 2.

The water used in this study was deionized and deaerated before adding the surfactant.

The porous medium, placed vertically to avoid buoyancy effects, was saturated under vacuum, then flushed by the foaming solution to equilibrate the adsorption of surfactant molecules on the pore walls. This adsorption was considered to be achieved after the time necessary to inject two pore volumes.

For all the experiments described here below, nitrogen was injected alone in the core at a fixed flow-rate value (0.5 ml/min) corresponding to a Darcy velocity of 35 cm/day. Gas injection was stopped after liquid water production dries up, which correspond to an injected volume of two pore volumes.

2.3. Experimental results

As mentioned before, we focused our attention on the influence of two physical parameters on foam flow in porous media, the influence of surfactant concentration and gas-flow rate which are, according to the literature, known to modify foam texture.

2.3.1. Influence of surfactant concentration

The experimental results, are analyzed in terms of breakthrough time (BT), liquid recovery, pressure drop along the whole core, and saturation profiles. All these experiments were performed at the same value of gas flow rate, 0.5 ml/min corresponding to a Darcy velocity of 35 cm/day.

The surfactant concentration values (mass fraction of active weight) are ranging from 0. to 1.0%.

2.3.1.1. Breakthrough time. The evolution of breakthrough time as a function of surfactant concentration is plotted in Fig. 3. In a first stage, we observe an increase of the breakthrough time until a value of the

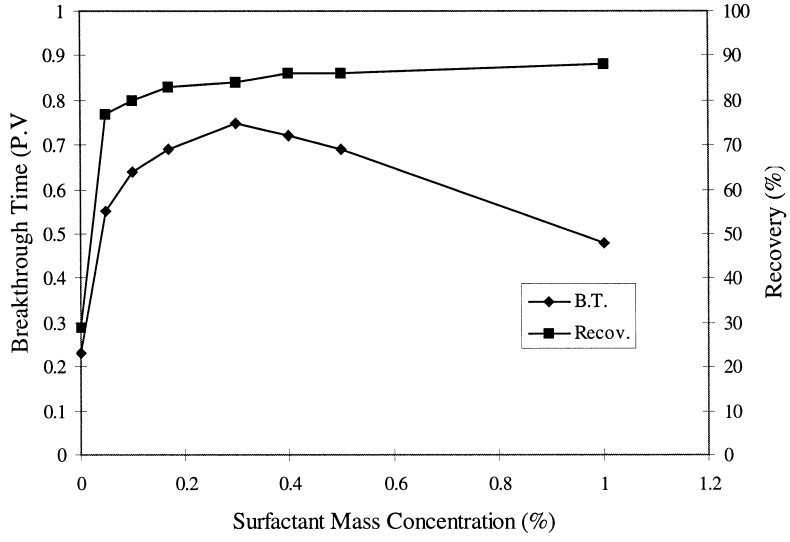

Fig. 3. Breakthrough time and final water recovery vs. surfactant mass concentration.

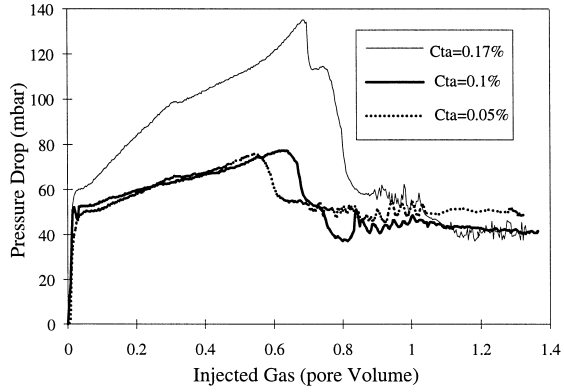

Fig. 4. Pressure drop vs. injected gas volume ($q = 0.5$ ml/min).

concentration equal to 0.3%. This behavior can be attributed to: (i) a modification of the mobility ratio leading to a better sweep of the medium, and, (ii) in a minor way, a modification of the capillary pressure due to the decrease of the surface tension (see Fig. 2) leading to a straightening-up of the displacement front.

When surfactant concentration becomes greater than 0.3%, breakthrough time decreases slightly. This behavior will be commented later with the observation of saturation profiles.

2.3.1.2. Final liquid recovery. The final liquid recovery, plotted in Fig. 3, increases rapidly when adding surfactant in the water and then, stays almost constant, contrary to the breakthrough time, when the surfactant concentration increases significantly.

2.3.1.3. Pressure drop. The pressure drop evolutions are reported in Figs. 4–6. The different observed behaviors can be analyzed in the following way. We can distinguish, in the range of surfactant concentration studied, three behavior groups corresponding to (i) low concentration values, lower than the CMC, represented in Fig. 4, (ii) concentration values contained between the CMC and almost two times the CMC (Fig. 5), and, (iii) high values of concentration (Fig. 6).

The evolution of the pressure drops represented in Figs. 4–6 show, in a first stage, a rapid increase, corresponding to foam generation at the inlet of the porous medium, then, foam propagation leads to a slight increase of the pressure drop until breakthrough. The increase in the pressure drop can be classically attributed to the progressive replacement of a more mobile phase by a less mobile phase, thus confirming the foaming

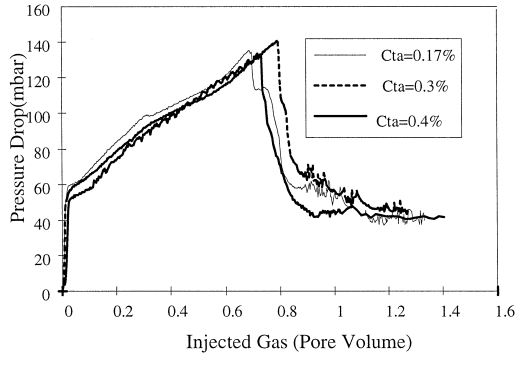

Fig. 5. Pressure drop vs. injected gas volume ($q = 0.5$ ml/min).

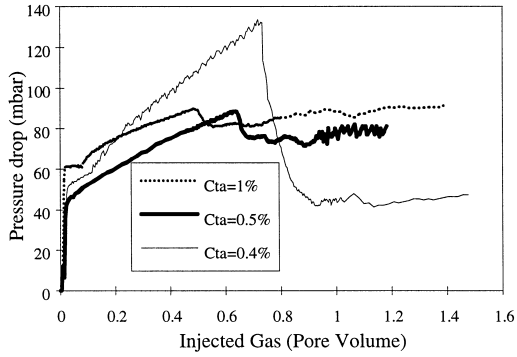

Fig. 6. Pressure drop vs. injected gas volume ($q = 0.5$ ml/min).

behavior. However, this interpretation assumes a 1-D displacement, which has to be discussed with respect to the observed saturation fields. Subsequently, in a second stage, a quasi-steady state is reached. Differences due to surfactant concentration levels are noticeable. In Fig. 4, for concentration $C = 0.05\%$ and $C = 0.1\%$, behaviors are the same except in terms of breakthrough time.

For C between the CMC and $C = 0.4\%$ (Fig. 5), the pressure drop slope corresponding to the foam propagation stage, is straighter, then there is a sharp decrease before reaching a quasi steady-state. This behavior is characteristic of a displacement with strong mobility control.

For concentrations above 0.4% (Fig. 6), the behavior starts to change. Before breakthrough, the pressure drop slope becomes weaker, while 'steady-state' pressure drop level increases with concentration after breakthrough. The 'excess' of surfactant leads to a weaker mobility control before breakthrough, which is corroborated by the decrease of breakthrough time reported above.

2.3.1.4. Saturation profiles. The 2D saturation maps (Fig. 7) measured during the displacement of pure water by gas show clearly the instability of the displacement front due to high viscosity contrast between the two phases.

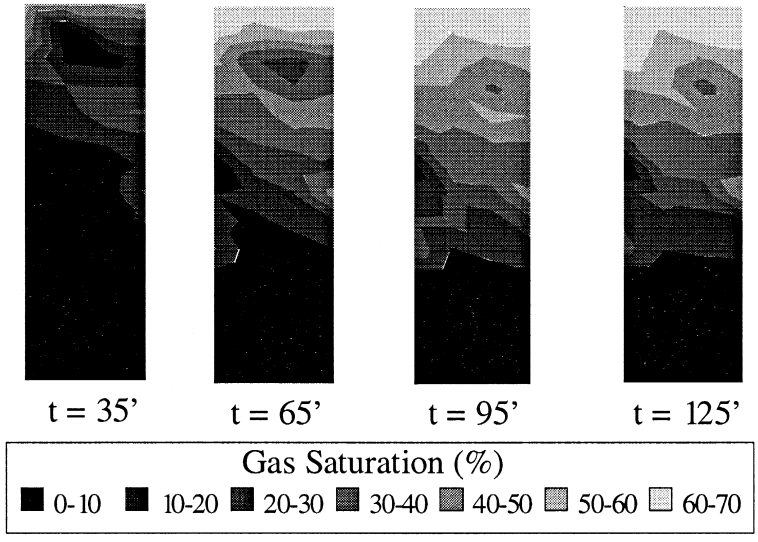

Fig. 7. Two-dimensional gas saturation fields ($C = 0\%$).

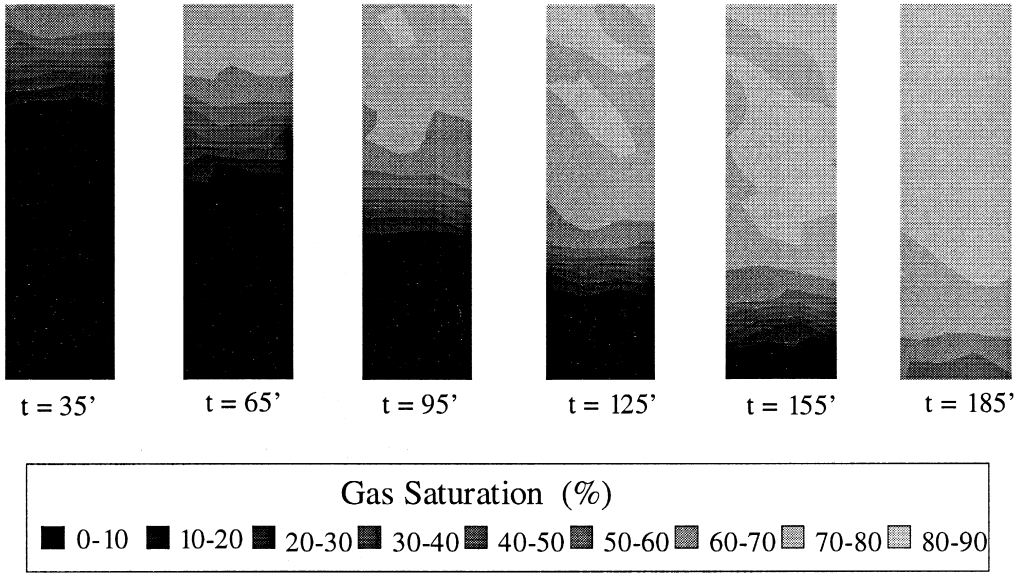

Fig. 8. Two-dimensional gas saturation fields ($C = 0.05\%$).

The saturation field stays almost constant after the breakthrough, indicating that gas is flowing through a preferential channel. In Fig. 8, we plotted the 2D saturation maps corresponding to the injection of gas into the porous medium saturated by a 0.05% surfactant solution. We see clearly the enhancement of sweeping efficiency due to a more favorable mobility ratio.

In Figs. 9 and 10, we plotted the evolution of the 1-D saturation averaged over a row of the grid points measurement. For a surfactant concentration lower than 0.4% (Fig. 9), there is almost no significant modification after the gas breakthrough. But, for surfactant concentrations values greater than 0.5% (Fig. 10),

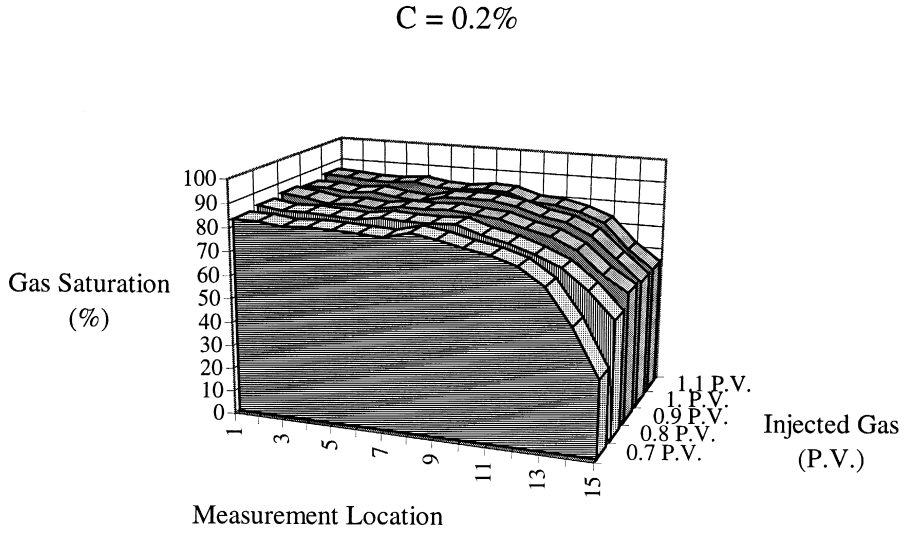

Fig. 9. One-dimensional gas saturation profiles after breakthrough ($C = 0.2\%$).

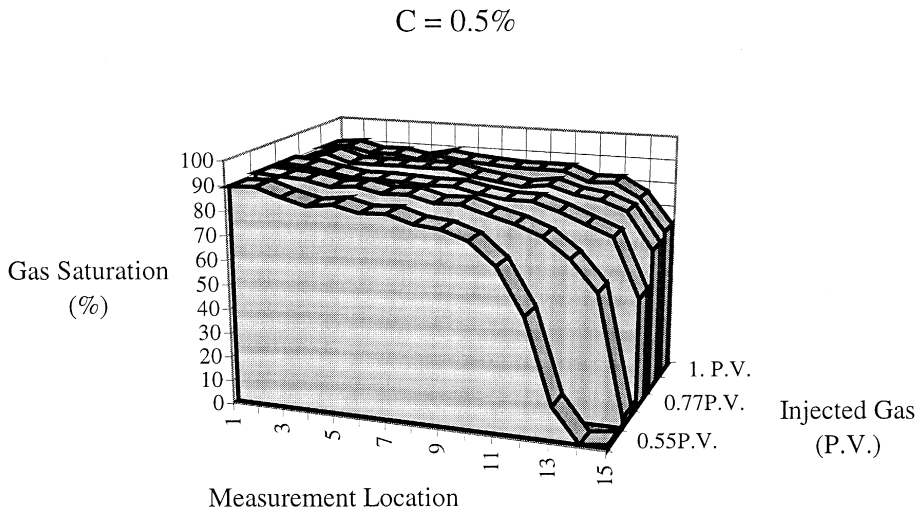

Fig. 10. One-dimensional gas saturation profiles after breakthrough ($C = 0.5\%$).

we notice a slight modification of the saturation profiles corresponding to a foam propagation that continues after the gas breakthrough. This means that lamellae are still generated after gas breakthrough; therefore, foam becomes stronger when surfactant concentration increases. However, the final recovery does not change significantly due to the fact that breakthrough time was shorter.

2.3.2. Influence of gas flow rate

As reported in the literature, gas velocity has a strong influence on foam texture. We report here below experiments performed at different gas flow rates for two values of the surfactant concentration, $C = 0.1\%$ and $C = 0.2\%$, corresponding to two different behaviors that can be identified as 'weak' and 'strong' foams as previously discussed.

2.3.2.1. $C = 0.1\%$. In Fig. 11, we plotted the evolution of the pressure drop measured along the core for two different values of the gas flow rate. As flow rate increases, gas breakthrough appears early. Nevertheless, pressure drop, in the first stage of the experiment, is sensibly the same for the two gas velocities. After gas breakthrough, for both experiments, we reach a steady-state regime. These experiments show clearly the non-Newtonian nature of the foam, and the destabilization, due to film breaking, of foam when gas velocity increases.

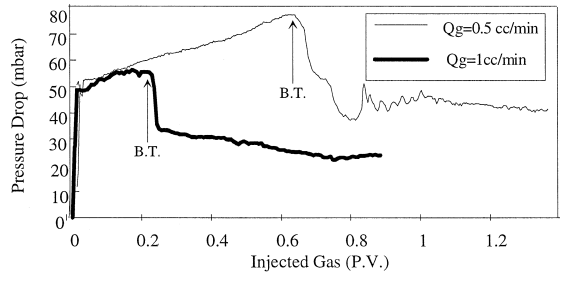

Fig. 11. Pressure drop vs. injected gas volume ($C = 0.1\%$).

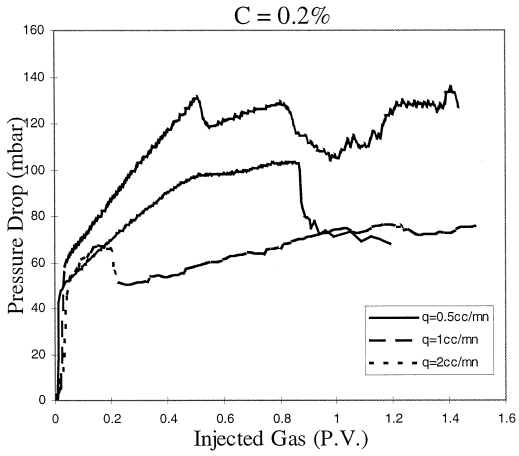

Fig. 12. Pressure drop vs. injected gas volume ($C = 0.2\%$).

2.3.2.2. C = 0.2%. In Fig. 12, we plotted the pressure drops for three different gas flow rates corresponding to frontal velocities of 0.35, 0.70 and 1.42 m/day. For gas flow-rates of 0.5 and 1 ml/min, the global behaviors are quite similar, although gas breakthrough decreases slightly when gas flow-rate increases.

For a gas flow-rate of 2 ml/min, we observe a very early gas breakthrough, and after, a constant increase of the pressure drop, indicating that foam is still generated and transported in the porous medium.

The difference of behaviors due to gas flow rate increase is emphasized in Figs. 13 and 14, where we plotted the averaged 1-D saturation profiles. Note that, due to the gas velocity increase, we reduced the measurement points number for the sake of accuracy. In Fig. 13, we see a regular sharp front gas displacement until breakthrough (BT = 0.71 PV), after breakthrough saturation profile modifications are small meaning that foam displacement is achieved. In Fig. 14, corresponding to a higher value of the flow rate, we see clearly the early gas breakthrough that occurs after 0.25 gas pore volume injected. However, foam continues to be generated (as

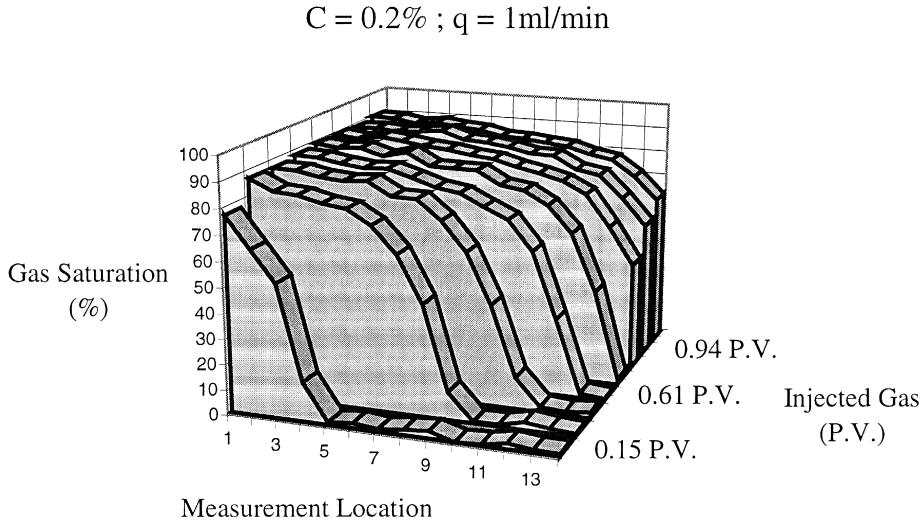

Fig. 13. One-dimensional gas saturation profiles ($C = 0.2\%$, $q = 1$ ml/min).

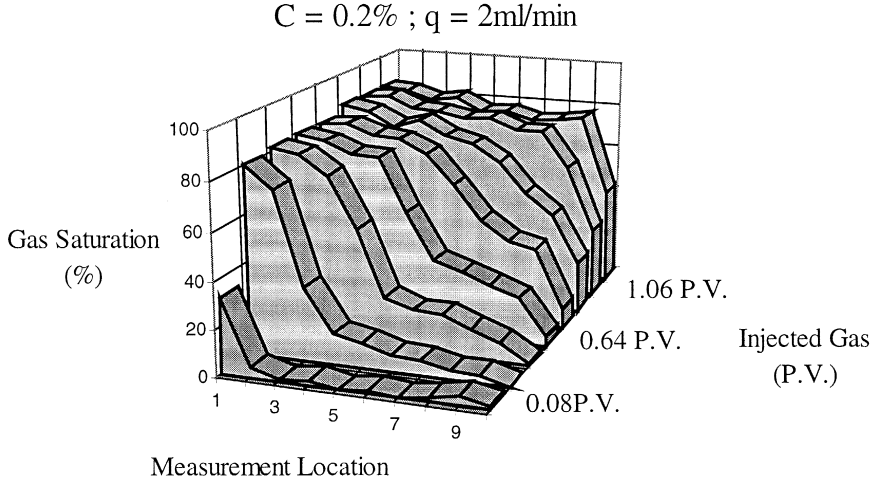

Fig. 14. One-dimensional gas saturation profiles ($C = 0.2\%$, $q = 2$ ml/min).

shown by the increase of the pressure drop) and transported in the porous medium (strong modification of the saturation profiles after gas breakthrough).

3. Foam displacement modeling

As reported in the literature, foam experiments performed at different scales of observation, pore-scale with micro-models, core-scale with homogeneous porous media, demonstrate clearly that foam texture is an important parameter that governs foam mobility. Therefore, in order to model foam displacement in porous media, it is necessary to take into account an external parameter into the generalized Darcy's laws, namely foam texture. Foam texture is characterized by the number of gas bubbles or lamellae, taking into account that all bubbles generated in the porous medium are not mobile. This can be achieved by using a population balance for the lamellae, which incorporates the mechanisms that generate or destroy the lamellae moving into the porous medium. Those mechanisms are, in the absence of oil, capillary snap-off, leave-behind and lamellae division for foam generation, and gas-diffusion and film breaking (bubble coalescence) for foam destruction.

Patzek (1988), Friedmann et al. (1988), Kovscek and Radke (1993) incorporated the population balance into conventional generalized Darcy's law models using experimental correlations to describe bubble generation and coalescence.

There are several other models in the literature dedicated to foam modeling in porous media. The simplest way consists in drawing up an experimental correlation between the gas mobility and the physical parameters influencing it, namely the surfactant concentration, the gas velocity, the saturation and the permeability. Then the flow is simulated using a conventional simulator (Islam and Farouq-Ali, 1990). Fisher et al. (1990) and Zhou and Rossen (1992) have developed models based on the concept of limiting capillary pressure, meaning that foam can be stable only if capillary pressure does not exceed a critical value allowing the existence of a stable thin film. In this approach, the limiting capillary pressure gives the corresponding saturation, and then the system of equations can be solved using the fractional-flow theory. An alternative way to simulate foam flow in porous media is to consider gas relative permeability reduction due to foam lamellae blockage. In this approach, gas relative permeability can be evaluated using percolation theory (Chou, 1990) or lattice models (Laidlaw et al., 1993).

There is a major difference between these models and the population-balance model, which deserves some discussion. The population-balance model does not presuppose the existence of a one- to-one relation between foam texture and the relevant parameters, namely surfactant concentration and velocity. Since it is usually acknowledged that mobility depends on the foam texture, the capability of models that do not contain this parameter to correctly model foam displacement is, in general, questionable. Their relative success may be due to the fact that correlations are determined and used in a limited parameter range for which extrapolations are valid. In principle, a population balance model has some advantage, since foam texture is part of the system description. However, the balance equation for lamellae density requires the introduction of several correlations describing foam generation and coalescence. In addition, other parameters in the momentum balance equations must be non-linear functions of the lamellae density. While this has been recognized as the major and fundamental advantage of the population balance model, its practical implementation is not straightforward, since the experimental determination of lamellae densities is not an easy task. This point deserves further investigations, which are beyond the scope of this paper. In this paper, we adopted the method put forward by previous investigators: required correlations are estimated from simple mechanistic models such as flow of lamellae in capillaries.

3.1. Population balance model

The population balance equation (Patzek, 1988), can be written in the form of the sum of accumulation plus advective terms equal to generation minus destruction terms

$$\varepsilon S_g \frac{\partial}{\partial t}\left[x_f n_f + (1 - x_f) n_t \right] + \nabla.(n_f \mathbf{u}_g) = \varepsilon S_g \left[G_f(\mathbf{v}_g) - C_f(n_f, P_c, \mathbf{v}_g) \right] \quad (5)$$

where S_g is the gas saturation, G_f and C_f are the bubble generation and coalescence terms, x_f is the gas flowing fraction, n_f and n_t are the flowing and total density of lamellae, $\mathbf{u}_g$ and $\mathbf{v}_g$ are the Darcy and interstitial gas velocities. As reported in the literature, G_f is a function of the local gas velocity only, whereas the coalescence rate is a function of the gas velocity, the capillary pressure and the number of flowing lamellae. In Eq. (5), some terms must be estimated using correlations developed in the literature to evaluate generation and destruction terms. These correlations are reported in the papers dealing with foam simulation using similar methods (Friedmann et al., 1988; Chang et al., 1990; Kovscek and Radke, 1994). Considering the results obtained in the last cited paper, we choose to take similar correlations.

3.1.1. Gas flowing fraction

$$x_f = \text{constant} \quad (6)$$

3.1.2. Lamellae generation

The lamellae are generated by snap-off or leave-behind phenomena, and the main parameters influencing the generation are the interstitial gas and water velocities

$$G_f = k_g v_g^{1/3} v_w \quad (7)$$

where k_g is the generation parameter.

3.1.3. Coalescence term

The coalescence of two bubbles is mainly due to: (i) gas diffusion through the lamellae and (ii) lamellae breaking; the coalescence term is taken proportional to the interstitial gas velocity and the flowing lamellae density,

$$C_f = k_c v_g n_f \quad (8)$$

where the coalescence parameter k_c, is a function of water saturation, defined in the following way,

$$k_c = k_c^0 \left(\frac{1 - S_w}{1 - S_w^*} \right) \tag{9}$$

where S_w^* is the critical water saturation corresponding to the critical (limiting) capillary pressure (Khatib et al., 1988).

3.1.4. Foam viscosity

Following the study of Hirasaki and Lawson (1985) dealing with foam rheology in capillary tubes, the viscosity of the foam (μ_f) depends on: (i) the density of mobile lamellae, and (ii) the gas velocity

$$\mu_f = \mu_g + \frac{\alpha n_f}{v_g^{1/3}} \tag{10}$$

where ε is a viscosity parameter function of the permeability.

The conservation equations for water and gas phases are written in the following way,

$$\frac{\partial}{\partial t}(\varepsilon S_w \rho_w) + \nabla.(\mathbf{u}_w \rho_w) = 0 \tag{11}$$

$$\frac{\partial}{\partial t}(\varepsilon S_g \rho_g) + \nabla.(\mathbf{u}_g \rho_g) = 0 \tag{12}$$

where S_w, ρ_w and $\mathbf{u}_w$ are the, saturation, density and Darcy velocity for the water phase. Similar definitions apply for the gas phase.

The generalized Darcy's laws are:

$$\mathbf{u}_w = \frac{k_{rw}}{\mu_w} \boldsymbol{K}.(\nabla P_w - \rho_w \mathbf{g}) \tag{13}$$

$$\mathbf{u}_g = \frac{k_{rg}}{\mu_g} \boldsymbol{K}.(\nabla P_g - \rho_g \mathbf{g}) \tag{14}$$

where $\boldsymbol{K}$ is the effective permeability, k_{rw} and k_{rg} are the relative permeabilities of water and gas. P_w and P_g are the water and gas pressures.

The relative permeability curves are expressed in Corey's form

$$k_{rw} = k_{rw}^0 \left[\frac{S_w - S_{wr}}{1 - S_{wr}} \right]^{n_1} \tag{15}$$

$$k_{rg} = k_{rg}^0 \left[1 - \frac{S_w - S_{wr}}{1 - S_{wr}} \right]^{n_2} \tag{16}$$

where S_{wr} is the residual water saturation (after gas drainage).

In addition, we consider that the relative permeability to the gas in the presence of foam is a function of the relative permeability to gas in the absence of foam through the flowing gas fraction,

$$k_{rg}^f(S_g) = x_f k_{rg}(S_g) \tag{17}$$

The system of equations is completed by the capillary pressure relationship

$$P_c = P_g - P_w \tag{18}$$

which can be expressed, by using the Leverett function,

$$Pc = \sigma(C)\left(\frac{\varepsilon}{\boldsymbol{K}}\right)^{1/2}\left(\frac{0.067}{S_w - S_{wr}}\right)^{0.2} \tag{19}$$

where σ is the interfacial tension.

In the case of injection of a surfactant slug, it is necessary to add a dispersion equation to express the surfactant concentration evolution,

$$\varepsilon\frac{\partial}{\partial t}(S_w C) + \nabla.(\mathbf{u}_w C) = \nabla.(D.\nabla C) \tag{20}$$

where C is the surfactant mass concentration and D the dispersion coefficient.

The general problem is written in 1-D, the initial condition corresponds to a constant water saturation along the core,

$$S_w = 1 \qquad 0 < x < L \tag{21}$$

the flow of the two fluids is specified at the inlet side (constant value of the gas flow-rate, no water flow) and the pressure outside of the core is considered to be the same in the two phases (Aziz and Settari, 1979) that leads to capillary pressure maintained to zero at the outlet side.

$$q_g = q_0 \ at\ x = 0 \tag{22}$$

$$P_c = 0 \ at\ x = L \tag{23}$$

The population balance equation is solved using an explicit scheme, while the conventional generalized Darcy's law model is solved using the IMPES method (Aziz and Settari, 1979).

The main difficulty is the choice of the different parameters values appearing in the correlations in the population balance. In the following, we focus our attention on one experiment performed at a constant gas flow rate of 0.5 ml/min with a surfactant-laden solution ($C = 0.1\%$).

3.2. Numerical simulations

The objective of this part is to study the influence of the different parameters occurring in the population-balance equation in order to obtain the best fit between the numerical and experimental results that are described in Part 2. The results are presented in terms of the whole pressure drop evolution and saturation profiles that can be easily compared to the experiments, and in terms of foam texture (density of lamellae). This last parameter, that has a strong influence on foam mobility is very difficult to quantify and could not be measured in our experiments.

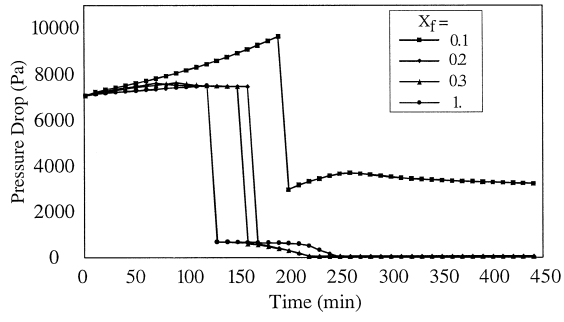

Fig. 15. Influence of flowing gas saturation on pressure drop.

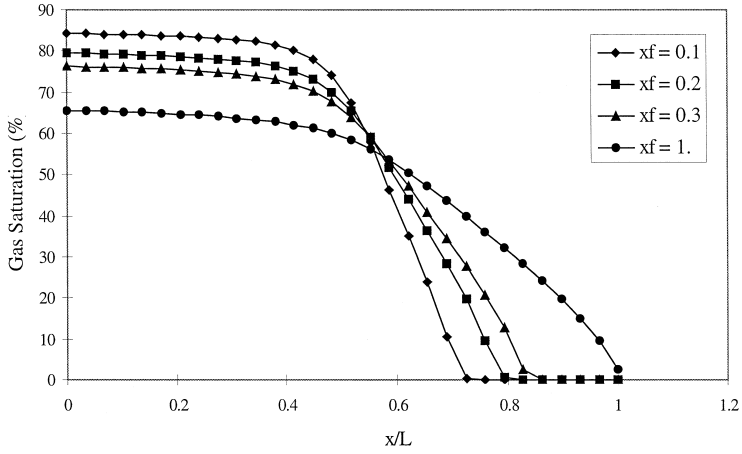

Fig. 16. Influence of flowing gas saturation on saturation profile at 0.5 PV.

3.2.1. Gas water displacement

In order to determine the relative permeability curves, we used the experimental results obtained for a pure water gas displacement. The best fitting of the pressure drop and saturation profiles has been obtained for the following parameters:

$$k_{rg}^{0} = 0.7;\ \ n_1 = 3;\ \ n_2 = 3;\ \ S_{wr} = 0.15.$$

3.2.2. Parameters sensitivity study

First of all, we choose a critical water saturation such as $S_w^* = 0.01$. This low value was chosen to ensure that flow occurs always in the lamellae generation regime.

3.2.2.1. Influence of the gas flowing fraction x_f. In this section, we settle the viscosity parameter, $\alpha = 2 \cdot 10^{-15}$ $\mathrm{Pa \cdot s^{2/3} \cdot m^{10/3}}$, the generation coefficient, $k_g = 1.10^8$ $\mathrm{m^{-13/3} \cdot s^{1/3}}$, and the coalescence coefficient, $k_c = 1$ $\mathrm{m^{-1}}$.

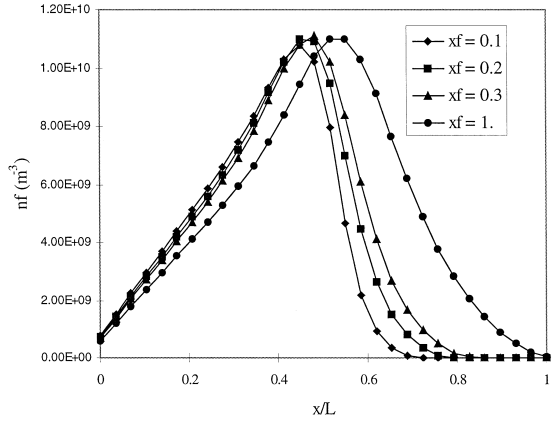

Fig. 17. Influence of flowing gas saturation on flowing lamellae density at 0.5 PV.

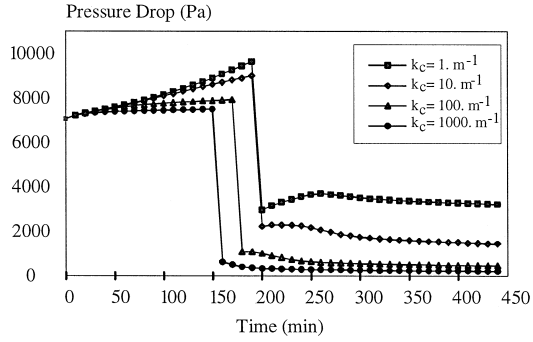

Fig. 18. Influence of coalescence coefficient on pressure drop.

When x_f is modified, the gas mobility is affected. This is well illustrated by the pressure drops plotted in Fig. 15, where we also observe the decrease of gas breakthrough with x_f increase. In Fig. 16, we plotted the saturation profiles corresponding to 0.5 pore volume injected for different values of x_f. We see clearly the 'spreading' of the displacement front due to the modification of the mobility ratio. The mobile lamellae density corresponding to 0.5 pore volume injected is represented in Fig. 17. The maximum density is almost the same whatever x_f values; however, a high gas flowing fraction gives a forward peak.

3.2.2.2. Influence of generation / coalescence ratio. Keeping constant the generation coefficient ($k_g = 1.10^8$ $m^{-13/3} \cdot s^{1/3}$) and the gas flowing fraction ($x_f = 0.1$), we screened the values of the coalescence coefficient k_c. The results are reported in Figs. 18–20. Increasing the coalescence coefficient has an obvious consequence on the pressure drop (Fig. 18), which is decreasing strongly when coalescence rate is high, i.e., a large k_c means that almost no foam is flowing. This is confirmed by the 'spreading' of the displacement front (Fig. 19) and the density of flowing lamellae (Fig. 20), which is very low when k_c is high.

3.2.2.3. Influence of the critical capillary pressure. The influence of the limiting capillary pressure is evaluated through the influence of the critical water saturation S_w^*. We had previously set this value to 0.01, which means that lamellae were always generated. Subsequently, the generation and coalescence coefficients have been set to

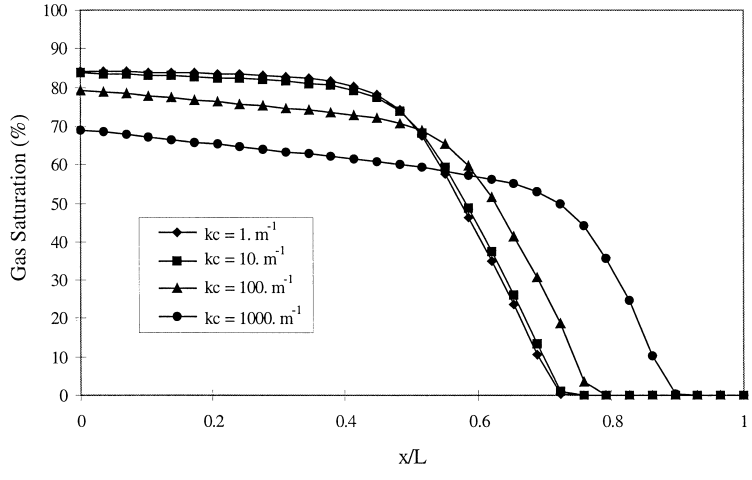

Fig. 19. Influence of coalescence coefficient on saturation profile at 0.5 PV.

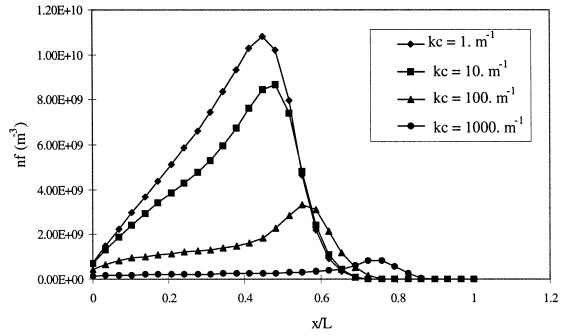

Fig. 20. Influence of coalescence coefficient on flowing lamellae density at 0.5 PV.

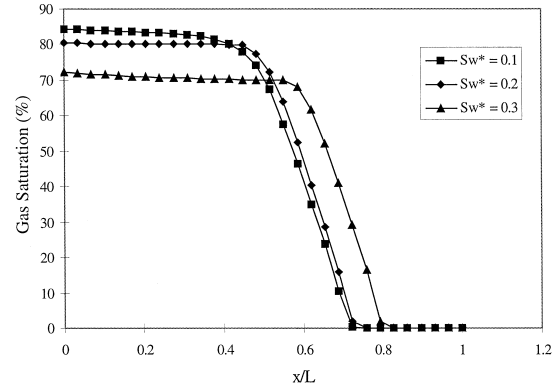

Fig. 21. Influence of limiting capillary pressure on saturation profile at 0.5 PV.

$1 \cdot 10^8$ $m^{-13/3} \cdot s^{1/3}$ and 1 m^{-1}, respectively. The influence of S_w^* on saturation profile (Fig. 21), at 0.5 pore volume injected, is weak, but, an increase of S_w^* has a strong influence on the flowing lamellae density (Fig. 22), reducing drastically the flowing bubbles number.

3.2.2.4. Optimal simulation. Since the parameters characteristic of the lamellae evolution cannot be measured directly, they must be estimated. A true optimization procedure represents a considerable effort that is beyond the scope of this paper. However, following the sensitivity study presented in the previous paragraphs, we choose a set of parameters susceptible to describe, at least qualitatively, the experimental data. We plotted in

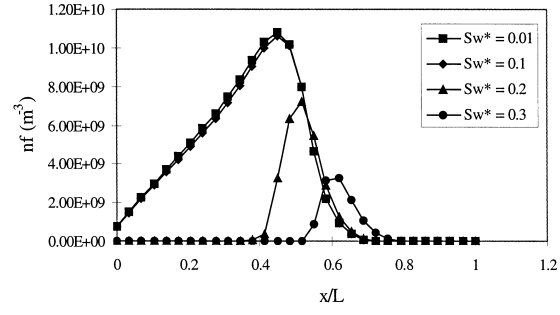

Fig. 22. Influence of limiting capillary pressure on flowing lamellae density at 0.5 PV.

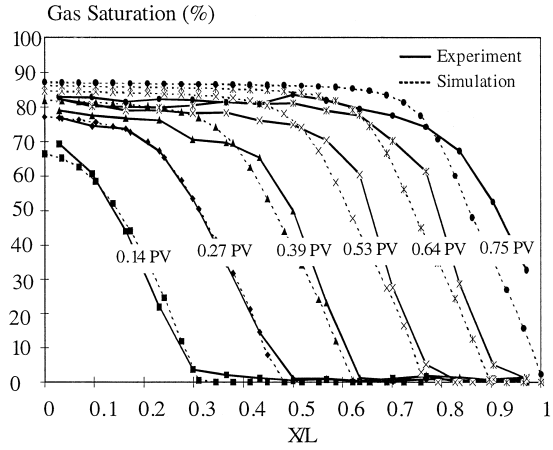

Fig. 23. Computed gas saturation profiles vs. experimental results ($C = 0.1\%$).

Figs. 23 and 24 the comparison between experimental and numerical results obtained for a surfactant concentration $C = 0.1\%$. Those results have been obtained for the following parameters:

$$x_f = 0.1; k_g = 1 \cdot 10^8\ \mathrm{m}^{-13/3} \cdot \mathrm{s}^{1/3}; k_c = 1\ \mathrm{m}^{-1}, \alpha = 2 \cdot 10^{-15}\ \mathrm{Pa} \cdot \mathrm{s}^{2/3} \cdot \mathrm{m}^{10/3} \text{ and } S_w^* = 0.1$$

The numerical simulation fits correctly the experimental saturation profiles (Fig. 23) while we observe, in Fig. 24, a difference in terms of the pressure drop amplitude. The whole qualitative behavior is satisfactorily described, i.e., foam propagation in a first stage then, after gas breakthrough, a steady state is reached. In Fig. 25, we plotted the evolution of the mobile lamellae density. We observe that n_f increases faster as we get closer to the outlet of the medium. This is due to the fact that we are always generating new lamellae that are transported along the porous medium.

Many reasons can be invoked to explain the discrepancy between the computed pressure drop and the actual data. These include uncertainty in the determination of the lamellae evolution parameters, as explained before, and also the lack of a correct reference for the relative permeability. In particular, Eq. (17) requires a correct evaluation of the gas relative permeability in the absence of foam, which is difficult to obtain because of channeling effects. However, only overall pressure drop has been measured, and not the pressure profile along the core that could have been worth for the comparison between experimental data and numerical results.

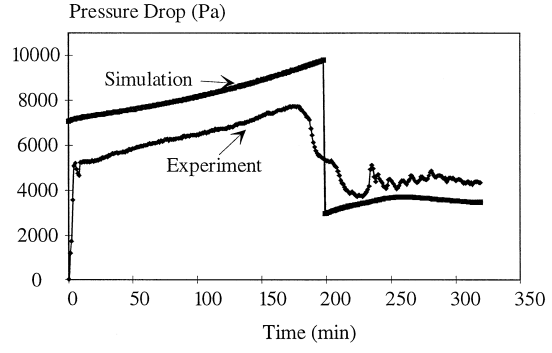

Fig. 24. Computed pressure drop vs. experimental results ($C = 0.1\%$).

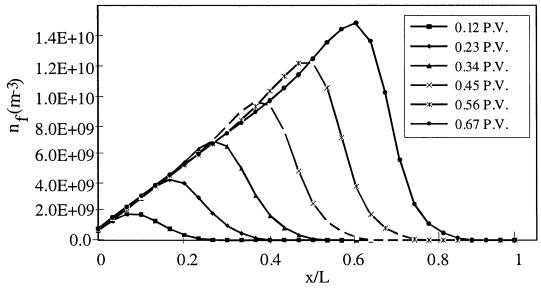

Fig. 25. Computed flowing lamellae density ($C = 0.1\%$).

Comparison between the optimal values set, (generation, coalescence and viscosity parameters) and the values published in the literature (Kovscek and Radke, 1994), shows a difference of magnitude. This discrepancy is due to the difference in terms of porous medium and surfactant used in the experiments.

Obviously, many experimental difficulties have to be overcome in order to set up an interpretation procedure that could go beyond the semi-quantitative comparison presented in this paper. However, the fact that simple mechanistic models give such fair predictions is promising in the sense that good starting estimates are available for a mathematically more sound parameter estimation.

4. Conclusions

The experimental study of transient aqueous foam flow in porous media, in the absence of oil, shows clearly the influence of surfactant concentration and gas velocity on gas mobility. For a low value of gas velocity, observation of gas breakthrough and pressure drop show the existence of different regimes of foam flow. When the gas flow rate increases, we observe, as a function of surfactant concentration, a modification of the gas mobility. If the lamellae are stable enough, an increase in the gas velocity allows a mobilization of a great number of lamellae that will reduce gas mobility. If the lamellae are unstable (low surfactant concentration), they will be destroyed leading to an increase of gas mobility.

The population balance equation provides a good mechanistic description of foam texture in porous media, taking into account the physical phenomenon that occurs at the pore level that govern generation and coalescence of gas bubbles. The modeling of transient aqueous foam flow provides results that are in good agreement with the experimental results. While parameters in the correlations are numerous and not easy to determine experimentally, there is some hope that convenient parameter estimation procedures can be implemented.

5. Nomenclature

C	Surfactant mass concentration
C_f	Coalescence rate (number of lamellae $m^{-3} \cdot s^{-1}$)
G_f	Generation rate (number of lamellae $m^{-3} \cdot s^{-1}$)
D	Dispersion coefficient ($m^2 \cdot s^{-1}$)

g	Gravity acceleration ($m \cdot s^{-2}$)
$\boldsymbol{K}$	Effective permeability (m^2)
k_c	Coalescence parameter (m^{-1})
k_g	Generation parameter (number of lamellae $m^{-13/3} \cdot s^{-1/3}$)
k_r	Relative permeability
l	Porous medium width (m)
L	Porous medium length (m)
n_1, n_2	Corey's exponents
n_f	Density of flowing lamellae (number of lamellae m^{-3})
n_t	Total density of lamellae (number of lamellae m^{-3})
N	Photon counting
P	Phase pressure (Pa)
P_c	Capillary pressure (Pa)
q	Flow rate ($m^3 \cdot s^{-1}$)
S	Phase saturation
$S*$	Critical saturation
t	Time (s)
$\mathbf{u}$	Darcy's velocity ($m \cdot s^{-1}$)
v	Interstitial velocity ($m \cdot s^{-1}$)
x	Coordinate (m)
x_f	Flowing gas fraction

Greek letters

α	Viscosity coefficient (Pa $s^{2/3} \cdot m^{10/3}$)
μ	Viscosity (Pa s)
ϑ	Porosity
ρ	Density ($kg \cdot m^{-3}$)
σ	Interfacial tension ($N \cdot m^{-1}$)
ζ	Linear attenuation coefficient (m^{-1})

Subscripts

d	Dry
f	Foam
g	Gas
0	Reference value
w	Water

Acknowledgements

This work has been supported by Institut Français du Pétrole (IFP) and Ecole Nationale Supérieure du Pétrole et des Moteurs. Special thanks to D. Defives and F. Kalaydjian for fruitful discussions. The authors thank the reviewers, whose comments were very helpful.

References

Aziz, K., Settari, A., 1979. Petroleum Reservoir Simulation. Applied Science Publishers, London.

Bergeron, V., Fagan, M.E., Radke, C.J., 1993. Generalized entering coefficients: a criterion for foam stability against oil in porous media. Langmuir 9 (7), 1704–1713.

Bond, D.C., Holbrook, O.C., 1958. Gas drive oil recovery process. US Patent No. 2,866,507.

Chambers, K.T., Radke, C.J., 1991. Capillary phenomena in foam flow through porous media. In: Morrow, N.R. (Ed.), Interfacial Phenomena in Petroleum Recovery, Marcel Dekker, New York.

Chang, S.H., Owusu, L.A., French, S.B., Kovarik, F.S., 1990. The Effect of Microscopic Heterogeneity on co_2 Foam Mobility: Part 2. Mechanistic Foam Simulation. Paper SPE 20191 presented at the SPE/DOE Enhance Oil Recovery Symposium, Tulsa, OK, April 22–25.

Chou, S.I., 1990. Percolation Theory of Foam in Porous Media. Paper SPE/DOE 20239, presented at the seventh SPE/DOE Symposium on Enhanced Oil Recovery Symposium, Tulsa, OK, April 22–25.

Fisher, A.W., Foulser, R.W.S., Goodyear, S.G., 1990. Mathematical Modeling of Foam Flooding. Paper SPE/DOE 20195 presented at the seventh SPE/DOE Enhance Oil Recovery Symposium, Tulsa, OK, April 22–25.

Fried, A.N., 1961. Foam drive process for increasing the recovery of oil. Bureau of Mines Report of Investigation.

Friedmann, F., Jensen, J.A., 1986. Some Parameters Influencing the Formation and Propagation of Foams in Porous Media. Paper SPE 15087 presented at the 56th Cal. Reg. Meeting of the SPE, Oakland, CA, April 2–4.

Friedmann, F., Chen, W.H., Gauglitz, P.A., 1988. Experimental and Numerical Study of High Temperature Foam Displacement in Porous Media. Paper SPE 17357 presented at the SPE/DOE Enhance Oil Recovery Symposium, Tulsa, OK, April 17–20.

Friedmann, F., Chen, W.H. and Gauglitz P., 1991. Experimental and Simulation Study of High Temperature Foam Displacement in Porous Media. SPE Res. Eng. (Feb.) pp. 37–45.

Gillis, J.V., Radke, C.J., 1990. A Dual Gas Tracer Technique for Determining Trapped Gas Saturation During Steady Foam Flow in Porous Media. Paper SPE 20519, presented at the 65th Annual Technical Conference, New Orleans, LA.

Hanssen, J.E., Haugun, P., 1991. Gas Blockage by Non-Aqueous Foams. Paper SPE 21002 presented at the International Symposium on Oilfield Chemistry, Anaheim, CA, Feb. 20–22.

Hirasaki, G.J., Lawson, J.B., 1985. Mechanisms of foam flow through porous media: apparent viscosity in smooth capillaries. SPE J., April, pp. 176–190.

Islam, M.R., Farouq-Ali, S.M., 1990. Numerical Simulation of Foam Flow in Porous Media. J. Can. Petrol. Technol., July–Aug., pp. 47–51.

Khatib, Z.I., Hirasaki, G.J., Falls, A.H., 1988. Effects of capillary pressure on coalescence and phase mobilities in foams flowing through porous media. SPE Res. Eng. Aug., pp. 919–926.

Kovscek, A.R., Radke, C.J., 1993. A comprehensive description of transient foam flow in porous media. Paper DOE/NIPER presented at the Symposium on field application of foams for oil production, Bakersfield, CA, Feb. 11–12.

Kovscek, A.R., Radke, C.J., 1994. Fundamentals of foam transport in porous media. In: Schramm, L.L. (Ed.), Foams: Fundamentals and applications in the petroleum industry. Adv. Chem. Series, ACS 242, pp. 115–163.

Laidlaw, W.G., Wilson, W.G., Coombe, D.A., 1993. A lattice model of foam flow in porous media: a percolation approach. Transport Porous Media 11, 139–159.

Manlowe, D.J., Radke, C.J., 1990. A pore-level investigation of foam/oil interactions in porous media. SPE Res. Eng., Nov., pp. 495–502.

Owete, S.O., Brigham, W.E., 1987. Flow behavior of foam: A porous micromodel study. SPE Res. Eng., Aug., pp. 315–323.

Patzek, T.W., 1988. Description of foam flow in porous media by the population balance method. In: Smith, D.H. (Ed.), Surfactant Based Mobility Control Progress in Miscible Flood Enhanced Oil Recovery, ACS Symposium Series No. 373, pp. 326–341.

Schramm, L.L. (Ed.), 1994a. Foams: Fundamentals and Applications in the Petroleum Industry. Adv. Chem. Series, ACS 242.

Schramm, L.L., 1994b. Foam sensitivity to crude oil in porous media. In: Schramm, L.L. (Ed.), Foams: Fundamentals and Applications in the Petroleum Industry. Adv. Chem. Series, ACS 242.

Schramm, L.L., Turta, A.T., Novosad, J.J., 1990. Microvisual and Coreflood Studies of Foam Interactions with a Light Crude Oil. SPE paper 20197, presented at the 7th SPE Symposium on Enhanced Oil Recovery, Tulsa, OK, April 22–25.

Zerhboub, M., Ben-Naceur, K. Touboul, E., Thomas, R., 1994. Matrix acidizing: A novel approach to foam diversion. SPE Prod. Facilities, May, pp. 121–126.

Zhou, Z.H., Rossen, W.R., 1992. Applying Fractional Flow Theory to Foam Processes at Limiting Capillary Pressure. Paper SPE 24180 presented at the 8th SPE/DOE Symposium on Enhanced Oil Recovery, Tulsa, OK, April 22–24.